Millimeter-Wave MIMO Transmission for FBMC Systems With Lens Antenna Arrays

Ying Wang, Qiang Guo, Jianhong Xiang, *Member, IEEE*, and Yu Zhong

***Abstract*—Millimeterwave (mmWave) techniques will be a key enabler for wireless communications to achieve high data rates. Additionally, Filter Bank Multi-Carrier (FBMC) with good spectral properties has also been regarded as an important transmission technique for future wireless communications. In this letter, we design and analyze an FBMC-based mmWave Multiple-input Multiple-output (MIMO) system. Specifically, we first pre-code quadrature amplitude modulation symbols in time to ensure that the MIMO technique becomes simple in FBMC. Secondly, we determine the optimal subcarrier spacing by maximizing the signal-to-interference ratio. Finally, using a lens antenna array combined with a simple channel estimator, we transmit data to the receiver. Simulation results show that FBMC can effectively support multi-antenna and mmWave techniques, providing favorable efficiency and reliability. Furthermore, we also verify that Alamouti's space time block code can provide considerable diversity gain.**

***Index Terms*—mmWave, FBMC, time-domain precoding, lens antenna arrays.**

I. Introduction

THE next decade will see an explosion in wireless data volumes. Millimeter wave technique that can utilize the huge bandwidth of 30-300 GHz becomes an interesting solution. Millimeter wave has already been applied in several standards, e.g., 5G new radios, IEEE 802.11ad for wireless local area networks [1] and wireless personal area network [2], etc. The International Telecommunication Union's IMT-2020 project has identified Filter Bank Multi-Carrier (FBMC) as a candidate for 5G [3]. Thus, combining millimeter-wave Multiple-Input-Multiple-Output (MIMO) technique with Offset Quadrature Amplitude Modulation (OQAM)-based FBMC allows for higher data rates and better spectral properties.

FBMC employs a time-frequency localization prototype filter. Thus, it can significantly reduce out-of-band emissions and easily meet the demands of strict synchronization [4]. However, many scholars claim that FBMC cannot effectively meet the key requirements for 5G like multiple antennas and low-latency transmission [5], [6]. This is not generally true. As shown by the measurements of R. Nissel et al. [7] over the 60 GHz real world channel, multi-antenna and low-latency transmission is feasible in FBMC once the data symbols are precoded in time domain. C.-Y. Liu et al. [8] described a 60 GHz FBMC-OQAM baseband receiver with 8x parallel memory access. S. Srivastava et al. [9] described a channel estimation technique for millimeter wave hybrid MIMO-FBMC-OQAM systems. A. I. Perez-Neira et al. [10] proposed a scheme to combine FBMC-OQAM waveform with MIMO. P. Singh et al. [11] derived MMSE receiver for MIMO-FBMC-OQAM. Also, P. Singh et al. emphasized the superiority of FBMC-OQAM waveforms over Orthogonal Frequency Division Multiplexing (OFDM) in massive MIMO systems [12]. On the other hand, the complexity of combining FBMC with MIMO can be reduced by precoding in time [13]. And, the transmitting lens antenna array can steer the transmitted signal with a sufficiently separated angle of departure, while the receiving lens antenna array can focus the signal with a sufficiently separated angle of arrival to different subsets of receiving antennas [14]. Based on the above theory, we designed an FBMC-MIMO millimeter-wave system with lens antenna arrays. The main contributions are summarized below:

1) This letter provides a scheme to incorporate FBMC into millimeter-wave MIMO systems and integrate lens antenna arrays. Specifically, we first perform time-domain precoding for Quadrature Amplitude Modulation (QAM) symbols to ensure that the MIMO technique becomes simple in FBMC-OQAM. Secondly, we construct the FBMC-OQAM millimeter-wave MIMO transmission model and increase the carrier frequency to 60 GHz. Finally, we employ a lens antenna array to transmit the signal to the receiver.
2) We derive an expression for the optimal subcarrier spacing by maximizing the Signal-to-Interference Ratio (SIR). Altering the subcarrier spacing, we can identify the weakest constraints on Doppler spreading and delay spreading, thus obtaining the minimal level of Inter-Symbol Interference (ISI) and Inter-Carrier Interference (ICI). Based on this, we obtain the optimal subcarrier spacing by maximizing the SIR.
3) We adopt the Saleh-Valenzuela (SV) channel model, which is widely considered for millimeter waves, and the 3GPP "CDL-D" channel model to verify the stability of the system. The results show that the FBMC-MIMO millimeter-wave system can perform robustly in both single-path and multi-path transmission cases[1].

Received 9 December 2024; accepted 24 February 2025. Date of publication 4 March 2025; date of current version 19 March 2025. This work was supported in part by the Fundamental Research Funds for the Central Universities, China, under Grant 3072022CF0801, and in part by the Sichuan Provincial Key Laboratory of Agile Intelligent Computing Project Fund. The associate editor coordinating the review of this article and approving it for publication was Dr. Ziyang Cheng. *(Corresponding author: Jianhong Xiang.)*

Ying Wang, Qiang Guo, and Jianhong Xiang are with the College of Information and Communication Engineering, Harbin Engineering University, Harbin 150001, China (e-mail: wangyingstu@163.com; guoqiang@hrbeu.edu.cn; xiangjianhong@hrbeu.edu.cn).

Yu Zhong is with the China Electronic Technology Group (Cetc-10), Chengdu 610036, China (e-mail: jade.zhong@hotmail.com).

Digital Object Identifier 10.1109/LSP.2025.3547268

[1] The detailed code can be downloaded at https://www.sciencedirect.com/science/article/pii/S016516842400046X.

Notations: vec$\{\cdot\}$ denotes the column vectorization operation. $\Re\{\cdot\}$ and $\Im\{\cdot\}$ denote the extract real and imaginary part operations, respectively. $\circ$ and $\otimes$ denote the Hadamard and the Kronecker product, respectively.

II. System Model

In FBMC-OQAM, the real and imaginary parts of the transmitted QAM symbols are staggered by half a symbol period. Maximum spectral efficiency is ensured by compressing the time-frequency spacing, which leads to orthogonality holding only in the real domain and to more challenging applications of MIMO. However, through time-domain precoding, we can restore the biorthogonality of FBMC-OQAM (abbreviated as FBMC), making MIMO as simple as in OFDM [13], [15]. If $\tilde{x}_{l,k/2}$ denotes the QAM symbol transmitted at subcarrier position l and time position k, then the function $\mathbb{P}(\cdot)$ completes the time-domain precoding for $\tilde{x}_{l,k/2}$. In matrix algebra, the encoded symbol vector $\mathbf{x} = [x_{1,1}, \ldots, x_{L,K}]^T \in \mathbb{C}^{LK\times 1}$ can be expressed as

$$\mathbf{x} = \mathbb{P}\left([\tilde{x}_{1,1}, \ldots, \tilde{x}_{L,K/2}]^T\right), \tag{1}$$

where L and K denote the number of subcarriers and time symbols, respectively. The operational details of (1) can be found in (5) of [13]. For convenient description of millimeter-wave MIMO transmission in the FBMC system, we assume that the Base Station (BS) is equipped with M antennas, and that there are Q users, each with one antenna, or equivalently, one user with Q antennas. According to the typical millimeter-wave beam space MIMO system model [14], [16], the downlink received signal vector $\mathbf{r} = [r_1(t), \ldots, r_Q(t)]^T \in \mathbb{C}^{Q\times 1}$ can be expressed as

$$\mathbf{r} = \mathbf{H}^H\mathbf{s} + \mathbf{n}, \tag{2}$$

where $\mathbf{H} \in \mathbb{C}^{M\times Q}$ denotes the beam space millimeter-wave MIMO channel. $\mathbf{s} = [s_1(t), \ldots, s_M(t)]^T \in \mathbb{C}^{M\times 1}$ denotes the transmitted signal vector and $\mathbf{n} = [\mathrm{n}_1(t), \ldots, \mathrm{n}_Q(t)]^T \in \mathbb{C}^{Q\times 1}$ the additive Gaussian noise. Note that in practice, the signals are discrete. Thus, in discrete form of FBMC, the signal $s_m(t)$ transmitted by mth BS antenna is a sampled signal $\mathbf{s}_m \in \mathbb{C}^{N\times 1}$ with N sample values, denoted as

$$\mathbf{s}_m = \mathbf{G}_m\mathbf{x}_m, \tag{3}$$

where $\mathbf{G}_m = [\mathbf{g}_{1,1}, \cdots \mathbf{g}_{L,K}] \in \mathbb{C}^{N\times LK}$ denotes the base pulse matrix for the mth antenna, and the base pulse vector $\mathbf{g}_{l,k} \in \mathbb{C}^{N\times 1}$ contains N sample values. $\mathbf{x}_m \in \mathbb{C}^{LK\times 1}$ denotes the transmitted symbols of the mth BS antenna. According to (2), the received signal $\mathbf{r}_q \in \mathbb{C}^{N\times 1}$ of the qth user can be expressed as

$$\mathbf{r}_q = \sum_{m=1}^{M} h_{m,q}\mathbf{s}_m, \tag{4}$$

where $h_{m,q}$ is the (m,q)th element of $\mathbf{H}$. Assuming perfect time synchronization, the received symbols of the qth user can be obtained by matched filtering, i.e., $\mathbf{y}_q = \mathbf{G}_q^H\mathbf{r}_q$. Each user can perform pre-decoding on the received symbols $\mathbf{y} = [y_{1,1}, \ldots, y_{L,K}]^T \in \mathbb{C}^{LK\times 1}$ to obtain the data symbol vector $\tilde{\mathbf{y}} \in \mathbb{C}^{LK/2\times 1}$, denoted as

$$\tilde{\mathbf{y}} = \mathrm{i}\mathbb{P}(\mathbf{y}), \tag{5}$$

where $\mathrm{i}\mathbb{P}(\cdot)$ denotes the pre-decoding operation for $\mathbf{y} \in \mathbb{C}^{LK\times 1}$, see (6) in [13].

To formulate the spatial domain millimeter-wave MIMO channel, we consider the widely used SV channel model [17]. The channel vector $\bar{\mathbf{h}}_q \in \mathbb{C}^{M\times 1}$ between the M-antenna BS and the qth user can be expressed as

$$\bar{\mathbf{h}}_q = \sqrt{\frac{M}{N_p}}\sum_{n_p=1}^{N_p}\alpha_{q,n_p}\mathbf{\Lambda}\left(\varphi_{q,n_p}^{azi}, \varphi_{q,n_p}^{ele}\right), \tag{6}$$

where N_p denotes the number of resolvable paths. α_{q,n_p}, φ_{q,n_p}^{azi} and φ_{q,n_p}^{ele} denote the complex gain, azimuth and elevation angles for the n_pth path, respectively. $\mathbf{\Lambda}(\varphi_{q,n_p}^{azi}, \varphi_{q,n_p}^{ele})$ denotes the $M\times 1$ steering vector, which depends on the array geometry. Without loss of generality, we omit subscripts and consider Uniform Linear Arrays (ULA) and Uniform Planar Arrays (UPA). For ULA, the steering vector $\mathbf{\Lambda}(\cdot)$ is determined by only one angle, denoted as

$$\mathbf{\Lambda}_{\mathrm{ULA}}(\varphi) = \frac{1}{\sqrt{M}}\left[\mathrm{e}^{-\mathrm{j}2\pi d\sin(\varphi)\mathbf{m}/\lambda}\right], \tag{7}$$

where $\mathbf{m} = [-(M-1), -M+3, \ldots, M-1]^T$. λ denotes the carrier wavelength and $d = \frac{\lambda}{2}$ the antenna spacing [18]. For the widely considered UPA, $\mathbf{\Lambda}(\varphi^{azi}, \varphi^{ele})$ can be expressed as

$$\mathbf{\Lambda}_{\mathrm{UPA}}\left(\varphi^{azi}, \varphi^{ele}\right) = \frac{1}{\sqrt{M}}\left[\mathrm{e}^{-\mathrm{j}2\pi d\sin(\varphi^{azi})\sin(\varphi^{ele})\mathbf{m}_1/\lambda}\right] \otimes \left[\mathrm{e}^{-\mathrm{j}2\pi d\cos(\varphi^{ele})\mathbf{m}_2/\lambda}\right], \tag{8}$$

where $\mathbf{m}_1 = [-(M_1-1), -M_1+3, \ldots, M_1-1]^T$ and $\mathbf{m}_2 = [-(M_2-1), -M_2+3, \ldots, M_2-1]^T$. Note that $M = M_1\times M_2$. M_1 and M_2 denote the number of horizontal and vertical antennas, respectively.

The space-domain channel can be directly converted into a beam space channel by using a lens antenna array [19]. Mathematically, the Lens Antenna Array functions as a Discrete Fourier Transform (DFT) [20], [21]. For ULA and UPA, the beam space channel can be expressed as

$$\mathbf{h}_q = \sqrt{\frac{M}{N_p}}\sum_{n_p=1}^{N_P}\alpha_{q,n_p}\mathbf{U}\mathbf{\Lambda}\left(\varphi_{q,n_p}^{azi}, \varphi_{q,n_p}^{ele}\right), \tag{9}$$

where $\mathbf{U} \in \mathbb{C}^{M\times M}$ denotes the DFT matrix. For ULA, $\mathbf{U} = \frac{1}{\sqrt{M}}[\mathrm{e}^{-\mathrm{j}2\pi\psi_1\mathbf{m}}, \ldots, \mathrm{e}^{-\mathrm{j}2\pi\psi_M\mathbf{m}}]^H$ with $\psi_m = \frac{1}{M}(m - \frac{M+1}{2})$. For UPA, $\mathbf{U} = [\bar{\mathbf{\Lambda}}(\psi_1^{azi}, \psi_1^{ele}), \ldots, \bar{\mathbf{\Lambda}}(\psi_{M_1}^{azi}, \psi_{M_2}^{ele})]^H$ with

$$\bar{\mathbf{\Lambda}}\left(\psi_m^{azi}, \psi_m^{ele}\right) = \frac{1}{\sqrt{M}}\left([\mathrm{e}^{-\mathrm{j}2\pi\psi_m^{azi}\mathbf{m}_1}] \otimes [\mathrm{e}^{-\mathrm{j}2\pi\psi_m^{ele}\mathbf{m}_2}]\right)^H, \tag{10}$$

where $\psi_m^{azi} = \frac{1}{M_1}(m - \frac{M_1+1}{2})$ and $\psi_m^{ele} = \frac{1}{M_2}(m - \frac{M_2+1}{2})$. The FBMC millimeter-wave MIMO downlink transmission structure with lens antenna array is shown in Fig. 1. If we consider the case of low-latency communication with ordinary antennas and mobility, the channel $h_{m,q}$ will be replaced by a time-varying convolution matrix $\mathbf{H}_{m,q} \in \mathbb{C}^{N\times N}$ [22].

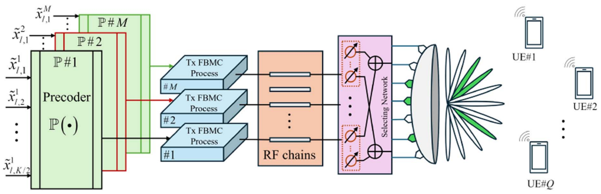

Fig. 1. FBMC millimeter-wave MIMO downlink transmission structure with Lens Antenna array.

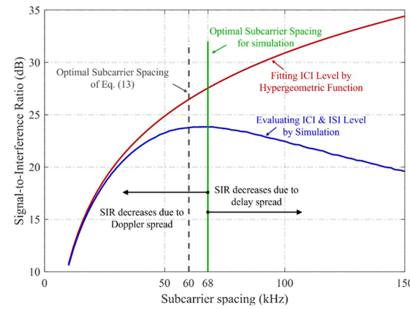

Fig. 2. SIR versus subcarrier spacing. Increasing the subcarrier spacing can improve the SIR. However, large subcarrier spacing leads to smaller symbol spacing, which causes Inter-Symbol Interference (ISI).

III. Optimal Subcarrier Spacing

The millimeter-wave band has abundant available bandwidth [23]. Also, the 5G new radio allows flexible allocation for subcarrier spacing, which makes subcarrier spacing a relevant factor for practical millimeter-wave systems. By increasing the subcarrier spacing, the ICI can be reduced, thereby improving the SIR of the system. For the classical Doppler spectrum, we can adopt a hypergeometric function to measure the ICI level for FBMC [24], expressed as

$$\mathrm{SIR}_{\mathrm{ICI}}^{\mathrm{FBMC}} = \frac{{}_1F_2\left(\frac{1}{2};\frac{3}{2},2;-(\frac{\pi\nu_{\max}}{F})^2\right)}{1-{}_1F_2\left(\frac{1}{2};\frac{3}{2},2;-(\frac{\pi\nu_{\max}}{F})^2\right)}, \tag{11}$$

where $\nu_{\max}$ denotes the maximum Doppler shift. As a rule of thumb, the chosen subcarrier spacing should ensure that the localization ratio is approximately equal to the spread ratio [25], denoted as

$$R_{\Delta} = \frac{\Delta_t}{\Delta_f} \approx \frac{\tau_{\mathrm{rms}}}{\nu_{\mathrm{rms}}}, \tag{12}$$

where Δ_t and Δ_f denote time localization and frequency localization, respectively. τ_{rms} and ν_{rms} denote Root Mean Square (RMS) delay spread and RMS Doppler spread, respectively. For the PHYDYAS pulse, $\Delta_t = \frac{0.2745}{F}$ and $\Delta_f = 0.328F$ [26]. Combined with (12), the subcarrier spacing F should be set as

$$F_{\mathrm{appx.,PHYDYAS}} \approx 0.91\sqrt{\nu_{\mathrm{rms}}/\tau_{\mathrm{rms}}}\,. \tag{13}$$

Unlike (13), we derive the SIR formulation for the mth antenna, implicitly assuming that all antennas use the optimal subcarrier spacing to maximize the SIR. Based on the base pulse matrix and channel information, we first calculate the base pulses correlation matrix $\mathbf{\Omega} \in \mathbb{C}^{LK\times LK}$ containing the channel gain, denoted as

$$\mathbf{\Omega} = \mathbf{G}_m^T\left(\mathbf{\Gamma}^H R_{h_{m,q}}\mathbf{\Gamma}\right)\mathbf{G}_m^* \quad st.\ \mathbf{\Gamma} = \mathbf{I}_{N\times N}\otimes \mathbf{g}_{l,k}, \tag{14}$$

where $R_{h_{m,q}} = h_{m,q}h_{m,q}^* \in \mathbb{C}^{1\times 1}$ denotes the channel correlation value. If $h_{m,q}$ is replaced by $\mathbf{H}_{m,q} \in \mathbb{C}^{N\times N}$, then $R_{h_{m,q}}$ becomes the channel correlation matrix $\mathbf{R}_{\mathbf{H}_{m,q}} \in \mathbb{C}^{N^2\times N^2}$, denoted as

$$R_{h_{m,q}} \triangleq \mathbf{R}_{\mathbf{H}_{m,q}} = \mathbb{E}\left\{\mathrm{vec}\{\mathbf{H}_{m,q}\}\mathrm{vec}\{\mathbf{H}_{m,q}\}^H\right\}. \tag{15}$$

Secondly, we need to perform phase compensation on $\mathbf{\Omega} \in \mathbb{C}^{LK\times LK}$ and extract the real part. The reason is that millimeter-wave FBMC is realized based on OQAM, and the phase shift factor is characterized in base pulses. Thus, the calculation of the SIR depends on the base pulse and requires phase compensation. On the other hand, although the FBMC can directly transmit precoded complex QAM symbols, the precoding does not change the properties of FBMC. Thus, the operation of extracting the real part for correlation matrix is also necessary. The compensation angle $\mathbf{\Xi} \in \mathbb{C}^{1\times LK}$ can be calculated as

$$\mathbf{\Xi} = \exp\left(-j\arctan\left(\frac{\Im\left\{[\mathbf{V}\sqrt{\mathbf{D}}]_{\ell,:}\right\}}{\Re\left\{[\mathbf{V}\sqrt{\mathbf{D}}]_{\ell,:}\right\}}\right)\right)$$
$$st.\ \mathbf{\Omega V} = \mathbf{VD}, \tag{16}$$

where $\ell = l + (k-1)L$. $\mathbf{V} \in \mathbb{C}^{LK\times LK}$ denotes the eigenvector matrix of $\mathbf{\Omega}$ and $\mathbf{D} \in \mathbb{C}^{LK\times LK}$ the eigenvalue matrix. The phase compensation and real part extraction operations can be expressed as

$$\bar{\mathbf{\Omega}} = \mathbf{V}\sqrt{\mathbf{D}} \circ (\mathbf{\Xi}\otimes \mathbf{1}_{LK\times 1}), \tag{17}$$

$$\mathbf{\Omega}_{\mathrm{OQAM}} = \Re\left\{\bar{\mathbf{\Omega}}\right\}\Re\{\bar{\mathbf{\Omega}}\}^H. \tag{18}$$

Finally, we can calculate the optimal subcarrier spacing $F_{\mathrm{opt.}}$ as

$$F_{\mathrm{opt.}} = \arg\max_F\ \{\mathrm{SIR}_m\}$$
$$st.\ \mathrm{SIR}_m = \frac{1}{LK}\sum_{\ell=1}^{LK}\frac{[\mathbf{\Omega}_{\mathrm{OQAM}}]_{\ell,\ell}}{\mathrm{Tr}\{\mathbf{\Omega}_{\mathrm{OQAM}}\} - [\mathbf{\Omega}_{\mathrm{OQAM}}]_{\ell,\ell}}. \tag{19}$$

Considering the "Extended Vehicular A" channel model with strong fading [27], we can simulate the SIR for different subcarrier spacings, see Fig. 2. Note that the RMS delay and Doppler spread for "Extended Vehicular A" are $\tau_{\mathrm{rms}} = 341$ns and $\nu_{\mathrm{rms}} = 1.57$ kHz, respectively. According to (13), we observe that the simulated maximum SIR is approximately 0.1 dB higher than the SIR corresponding to the subcarrier spacing in (13). Therefore, in this letter, we consistently use the subcarrier spacing that maximizes the SIR.

IV. Numerical Results

To evaluate the reliability of the millimeter-wave FBMC-MIMO system, we perform a series of simulation experiments. Unless otherwise stated, the simulation parameters are summarized in Table I.

Unlike low-frequency signals, millimeter-wave signals suffer from large attenuation due to high-frequency properties. Millimeter wave signals cannot be reliably transmitted in strong fading channels. Thus, the subcarrier spacing in Table I is

TABLE I
SIMULATION PARAMETERS

Parameters	Value
Carrier Frequency	60 GHz
Subcarrier spacing F	120 kHz
Number of subcarriers L	256
Number of time symbols in per frame K	16
Bandwidth FL	30.72 MHz
Sampling rate $15FL$	460.8 MHz
Constellation	4-QAM
Bit rate (ignoring pilot)	35.35 Mbit/s
No. of antennas M and users Q	64, 8
Number of resolvable paths N_p	10
Array Geometry	UPA
Prototype Filter, Overlap Factor	PHYDYAS, 4

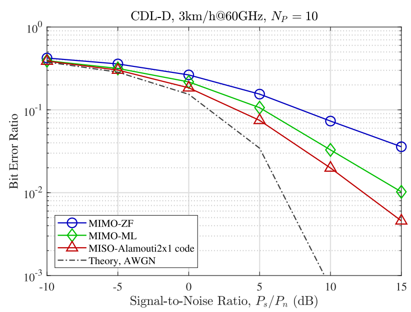

Fig. 3. BER performance for FBMC-MIMO millimeter-wave system with mobility in the case of low-latency indoor transmission (no lens antenna array assisted). P_s and P_n denote signal and noise power, respectively.

recalculated based on the adopted channel. Moreover, as shown in Table I, the bandwidth is only 30.72 MHz, which is much smaller than the 2.16 GHz bandwidth available for millimeter waves [28]. The reason is that the maximum sampling rate allowed by our equipment is about 500 MHz and lowering the sampling rate may result in signal distortion. However, there is no direct relationship between bandwidth and uncoded BER (i.e., without error-correcting codes) [7]. BER usually depends on the SNR of the received signal. In other words, as long as the same SNR is guaranteed under different bandwidths, the bandwidth has no effect on the uncoded BER.

For each user (or each received antenna), we consider a simple channel estimator, denoted as

$$\hat{h}_{m,q} = \mathbb{E}\left\{\mathbf{y}_{\mathcal{P}}^{m,q}/\mathbf{x}_{\mathcal{P}}^{q}\right\}, \tag{20}$$

where $\mathbf{y}_{\mathcal{P}}^{m,q}$ denotes the received pilot symbol at the qth antenna from the mth transmitted antenna. $\mathbf{x}_{\mathcal{P}}^{q}$ denotes the pilot symbol corresponding to the q th received antenna. In FBMC-MIMO millimeter-wave systems with lens antenna arrays, the normalized mean-square error for the channel estimator in (20) can reach -34 dB. Thus, we believe that the estimator of (20) is valid. On the other hand, we realize symbol detection by employing Zero Forcing (ZF) and Maximum Likelihood (ML) detection at the receiver. For the multipath, we adopt Alamouti's space time block code technique.

Considering ordinary multi-antenna transmission, Fig. 3 shows the BER performance of the FBMC-MIMO millimeter-wave system in the "CDL-D" [29] channel with a velocity of 3 km/h. This channel model provides a low-latency indoor Non-Line-of-Sight (NLOS) transmission case with mobility. We observed that the reliability of the system is greatly impacted despite the small mobility. This indicates that the FBMC-MIMO millimeter-wave signal fading is more serious than the low-frequency FBMC signals. Further, we observe that Alamouti's space time block code provides diversity gain. Since the number of resolvable paths is set to 10, Alamouti's space-time block code utilizes spatial diversity, thereby improving the reliability of the system.

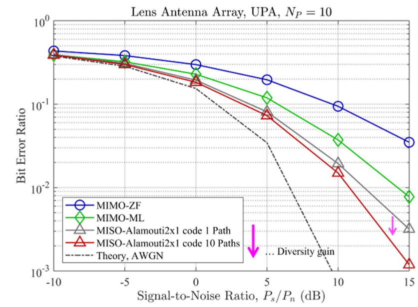

Fig. 4. BER performance for FBMC-MIMO millimeter-wave system in SV channel (with Lens Antenna Array assist).

Considering the multi-antenna transmission with Lens Antenna Array assist, Fig. 4 shows the BER performance for FBMC-MIMO millimeter-wave system in the SV channel. We observe that Alamouti's space time block code provides no diversity gain anymore in the one-path case. However, once the path number increases, Alamouti's space time block code provides diversity gain. On the other hand, the lens antenna array can focus and amplify the signal. Thus, FBMC-MIMO millimeter-wave systems with Lens Antenna Arrays are more reliable. For example, the performance of ZF and ML is improved by about 22.12% and 50.5% , respectively, and the performance of Alamouti's space time block code is improved by about 97.5% . Note that the BER is limited by the saturation effect of lens focusing and the channel separability. When the number of antennas and users increases excessively, the saturation effect of lens focusing intensifies, leading to focal spillover and insufficient signal diversity gain. Thus, the BER of the $64\times$ 8 system is higher than that of the $2\times$ 1 system.

V. CONCLUSION

This work investigates the performance of FBMC signaling in next-generation millimeter-wave communications. An architecture for incorporating FBMC into millimeter-wave MIMO systems is presented. We calculate the optimal subcarrier spacing by maximizing the SIR. At the receiver, we adopt a simple channel estimator and consider ZF equalization and ML detection to achieve symbol detection for the system. For multipath fading, we consider Alamouti's space time block code technique. Once the system has multiple paths, spatial diversity technique enhances the system reliability. Additionally, high subcarrier spacing reduces transmission time, leading to low-delay transmission. Therefore, FBMC-MIMO millimeter waves can fulfill 5G requirements. However, issues such as hardware mismatch and the intensified focusing saturation effect in larger-scale antenna systems for mmWave FBMC-MIMO still require further investigation.

REFERENCES

[1] C. Cordeiro, D. Akhmetov, and M. Park, "IEEE 802.11 ad: Introduction and performance evaluation of the first multi-Gbps WiFi technology," in *Proc. 2010 ACM Int. Workshop mmWave Commun., Circuits Networks*, 2010, pp. 3–8.

[2] F. Giannetti, M. Luise, and R. Reggiannini, "Mobile and personal communications in the 60 GHz band: A survey," *Wireless Pers. Commun.*, vol. 10, pp. 207–243, 1999.

[3] F. Rancy, "5G and" IMT for 2020 and beyond" [Spectrum Policy and Regulatory Issues]," *IEEE Wireless Commun.*, vol. 22, no. 4, pp. 2–3, 2015.

[4] A. Aminjavaheri, A. Farhang, A. RezazadehReyhani, and B. Farhang-Boroujeny, "Impact of timing and frequency offsets on multicarrier waveform candidates for 5G," in *Proc. IEEE Signal Process. Signal Process. Educ. Workshop*, 2015, pp. 178–183.

[5] C. Lélé, P. Siohan, and R. Legouable, "The alamouti scheme with CDMA-OFDM/OQAM," *EURASIP J. Adv. Signal Process.*, vol. 2010, pp. 1–13, 2010.

[6] R. Nissel, E. Zochmann, and M. Rupp, "On the influence of doubly-selectivity in pilot-aided channel estimation for FBMC-OQAM," in *Proc. IEEE 85th Veh. Technol. Conf.*, 2017, pp. 1–5.

[7] R. Nissel, E. Zöchmann, M. Lerch, S. Caban, and M. Rupp, "Low-latency MISO FBMC-OQAM: It works for millimeter waves!," in *Proc. 2017 IEEE MTT-S Int. Microw. Symp.*, 2017, pp. 673–676.

[8] C. -Y. Liu et al., "An 8X-parallelism memory access reordering polyphase network for 60 GHz FBMC-OQAM baseband receiver," *IEEE Trans. Circuits Syst. I, Reg. Papers*, vol. 63, no. 12, pp. 2347–2356, Dec. 2016.

[9] S. Srivastava, P. Singh, A. K. Jagannatham, A. Karandikar, and L. Hanzo, "Bayesian learning-based doubly-selective sparse channel estimation for millimeter wave hybrid MIMO-FBMC-OQAM systems," *IEEE Trans. Commun.*, vol. 69, no. 1, pp. 529–543, Jan. 2021.

[10] A. I. Pérez-Neira et al., "MIMO signal processing in offset-QAM based filter bank multicarrier systems," *IEEE Trans. Signal Process.*, vol. 64, no. 21, pp. 5733–5762, Nov. 2016.

[11] P. Singh, R. Budhiraja, and K. Vasudevan, "Probability of error in MMSE detection for MIMO-FBMC-OQAM systems," *IEEE Trans. Veh. Technol.*, vol. 68, no. 8, pp. 8196–8200, Aug. 2019.

[12] P. Singh, H. B. Mishra, A. K. Jagannatham, K. Vasudevan, and L. Hanzo, "Uplink sum-rate and power scaling laws for multi-user massive MIMO-FBMC systems," *IEEE Trans. Commun.*, vol. 68, no. 1, pp. 161–176, Jan. 2020.

[13] Y. Wang, Q. Guo, J. Xiang, L. Wang, and Y. Liu, "Bi-orthogonality recovery and MIMO transmission for FBMC systems based on non-sinusoidal orthogonal transformation," *Signal Process.*, vol. 219, 2024, Art. no. 109427. [Online]. Available: https://www.sciencedirect.com/science/article/pii/S016516842400046X

[14] Y. Zeng and R. Zhang, "Millimeter wave MIMO with lens antenna array: A new path division multiplexing paradigm," *IEEE Trans. Commun.*, vol. 64, no. 4, pp. 1557–1571, Apr. 2016.

[15] R. Nissel and M. Rupp, "Enabling low-complexity MIMO in FBMC-OQAM," in *Proc. 2016 IEEE Globecom Workshops*, 2016, pp. 1–6.

[16] T. Xie, L. Dai, D. W. K. Ng, and C. -B. Chae, "On the power leakage problem in millimeter-wave massive MIMO with lens antenna arrays," *IEEE Trans. Signal Process.*, vol. 67, no. 18, pp. 4730–4744, Sep. 2019.

[17] A. Alkhateeb, O. El Ayach, G. Leus, and R. W. Heath, "Channel estimation and hybrid precoding for millimeter wave cellular systems," *IEEE J. Sel. Topics Signal Process.*, vol. 8, no. 5, pp. 831–846, Oct. 2014.

[18] S. Han, C. -l. I, Z. Xu, and C. Rowell, "Large-scale antenna systems with hybrid analog and digital beamforming for millimeter wave 5G," *IEEE Commun. Mag.*, vol. 53, no. 1, pp. 186–194, Jan. 2015.

[19] X. Wei, C. Hu, and L. Dai, "Deep learning for beamspace channel estimation in millimeter-wave massive MIMO systems," *IEEE Trans. Commun.*, vol. 69, no. 1, pp. 182–193, Jan. 2021.

[20] X. Gao, L. Dai, S. Han, C. -L. I, and X. Wang, "Reliable beamspace channel estimation for millimeter-wave massive MIMO systems with lens antenna array," *IEEE Trans. Wireless Commun.*, vol. 16, no. 9, pp. 6010–6021, Sep. 2017.

[21] X. Gao, L. Dai, and A. M. Sayeed, "Low RF-complexity technologies to enable millimeter-wave MIMO with large antenna array for 5G wireless communications," *IEEE Commun. Mag.*, vol. 56, no. 4, pp. 211–217, Apr. 2018.

[22] Y. Wang, Q. Guo, J. Xiang, and Y. Liu, "Doubly selective channel estimation and equalization based on ICI/ISI mitigation for OQAM-FBMC systems," *Phys. Commun.*, vol. 59, 2023, Art. no. 102120. [Online]. Available: https://www.sciencedirect.com/science/article/pii/S1874490723001234

[23] S. Kim and J. Verboom, "On the coexistence of WiGig and NR-U in 60 GHz band," in *Proc. IEEE 93rd Veh. Technol. Conf.*, 2021, pp. 1–5.

[24] P. Robertson and S. Kaiser, "The effects of doppler spreads in OFDM(A) mobile radio systems," in *Proc. Gateway 21st Century Commun. Village. VTC 1999-Fall. IEEE VTS 50th Veh. Technol. Conf. (Cat. No. 99CH36324)*, 1999, vol. 1, pp. 329–333.

[25] B. Farhang-Boroujeny, "OFDM versus filter bank multicarrier," *IEEE Signal Process. Mag.*, vol. 28, no. 3, pp. 92–112, May 2011.

[26] R. Nissel, S. Schwarz, and M. Rupp, "Filter bank multicarrier modulation schemes for future mobile communications," *IEEE J. Sel. Areas Commun.*, vol. 35, no. 8, pp. 1768–1782, Aug. 2017.

[27] 3rd Generation Partnership Project (3GPP), "Evolved Universal Terrestrial Radio Access (E-UTRA); User equipment (UE) radio transmission and reception," 3GPP, Sophia Antipolis, France, Tech. Specification 36.101, Dec. 2007. [Online]. Available: http://www.3gpp.org

[28] R. Heath, "Wearable networks: A new frontier for device-to-device communication," presented at WCNC, 2015. [Online]. Available: https://wdpc.fiu.edu/wp-content/uploads/2015/03/WDPC-Keynote-Panel-R.HEATH_.pdf

[29] 3rd Generation Partnership Project (3GPP), "Study on channel model for frequency spectrum above 6 GHz," 3GPP, Sophia Antipolis, France, Tech. Rep. 38.900, Jun. 2018. [Online]. Available: http://www.3gpp.org/DynaReport/38900.htm